



## Full length Article

# Transition of the Taiwan-Ryukyu collision-subduction process as revealed by ocean-bottom seismometer observations



Shao-Jinn Chin <sup>a,b</sup>, Jing-Yi Lin <sup>a,b,\*</sup>, Yen-Fu Chen <sup>a</sup>, Wen-Nan Wu <sup>c</sup>, Chin-Wei Liang <sup>a,b</sup>

<sup>a</sup> Department of Earth Sciences, National Central University, No. 300, Jhongda Rd., Jhongli City, Taoyuan 32001, Taiwan, ROC

<sup>b</sup> Center for Environmental Studies, National Central University, No. 300, Jhongda Rd., Jhongli City, Taoyuan 32001, Taiwan, ROC

<sup>c</sup> Institute of Earth Sciences, Academia Sinica, Nankang, Taipei 11529, Taiwan, ROC

## ARTICLE INFO

## Article history:

Received 1 March 2016

Received in revised form 14 June 2016

Accepted 10 July 2016

Available online 16 July 2016

## Keywords:

Arc-continental collision

Taiwan

Ocean Bottom Seismometer

Seismicity

Subduction

## ABSTRACT

Located at the arc-continental collision region between the Eurasian (EP) and Philippine Sea Plates (PSP), Taiwan is usually considered to have a complex tectonic environment, particularly along the eastern coast of the island. To gain a better understanding of the geological evolution of the east Taiwan area, the data from 8 Ocean Bottom Seismometers (OBS) acquired during the Across Taiwan Strait Explosion Experiment in 2012 and 14 inland seismic stations were used to determine a more detailed and accurate distribution of marine earthquakes. Based on the 333 relocated earthquakes and available geophysical data, we suggest two main tectonic boundaries for eastern Taiwan. South of 23.25°N, the homogeneous distribution of earthquakes in the crustal portion for both the inland and offshore areas suggests an ongoing collisional process. North of this location, between approximately 23.25°N and 23.8°N, the abrupt increasing of seismicity depth infers that the underthrust arc/fore-arc material is deforming due to the collisional compression at depth. In this segment, the subsidence of the arc/fore-arc area determines the transition from collision to subduction. North of 23.8°N, the northwestern dipping PSP is well illustrated by the seismicity both onshore and offshore, indicating a dominant subduction process.

© 2016 Elsevier Ltd. All rights reserved.

## 1. Introduction

Taiwan is located at the plate boundary between the Eurasian and the Philippine Sea Plates. Along the eastern coast of Taiwan, the Eurasian Plate (EP) subducts eastward under the Philippine Sea Plate (PSP) in the southern region, whereas the PSP subducts northward under the EP along the Ryukyu Trench (RT) (Fig. 1). In eastern Taiwan, the Longitudinal Valley Fault (LVF) is generally considered the suture zone. In addition, the Ryukyu subduction system enters eastern Taiwan from the offshore area and interacts with the northern Taiwan orogenic system. Subsequently, complex geological structures and abundant earthquakes occupy this area.

Several tectonic investigations have been performed to detail the tectonic characteristics of this complicated region. Based on analog sandbox experiments, Chemenda et al. (2001) showed that the progressively increasing compression of the overriding lithosphere causes the subduction of the fore-arc block and results in the subsidence of the arc and fore-arc. Malavieille et al. (2002) interpreted the marine seismic profiles and proposed that the

subduction of the EP induces the shortening of the fore-arc region and the accretion of regions of the arc with westward thrusting features. By analyzing the earthquake distribution and tomographic images, Lallemand et al. (2001) suggested the existence of a subvertical tear fault within the EP at the NE Taiwan offshore, which allows the northwest subduction of PSP. However, Ustaszewski et al. (2012) introduced an overturned EP according to a 3D velocity model interpolated from several 1D models. In addition to these controversy over the morphology of the two reversal plates, the boundary between the collision and northward subduction is also unclear. Based on geological data, Lu et al. (1995) suggested that the boundary extends from the western side of the Hoping Basin toward Suao and ends at approximately 24.5°N, constructing the model of the opening Taipei basin. Kao et al. (1998) defined the collision-subduction boundary at 24.2°N according to the distribution of focal mechanisms. By analyzing the seismicity and modulated GPS velocity data, Wu et al. (2009a) extended the discernible RT westward to the eastern coast of Taiwan at 23.5°N, suggesting an indenter model to interpret the transition from collision to subduction. Although numerous models have been suggested, many questions regarding the tectonic processes in eastern Taiwan remain unsolved. One of the main issues is that a large portion of the tectonic process is ongoing in the

\* Corresponding author at: Department of Earth Sciences, National Central University, No. 300, Jhongda Rd., Jhongli City, Taoyuan 32001, Taiwan, ROC.

E-mail address: [jylin.gep@gmail.com](mailto: jylin.gep@gmail.com) (J.-Y. Lin).

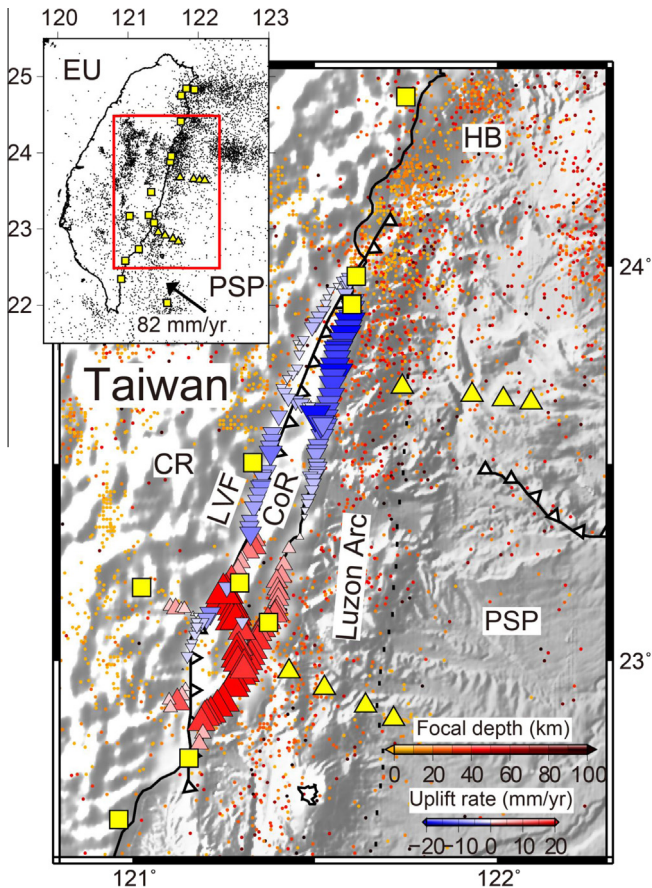


**Fig. 1.** Major tectonic structures and earthquake distribution in Taiwan area. The seismicity (colored dots) is from the reviewed International Seismological Center (ISC) catalog during 1990/1/1–2011/3/31 with magnitude larger than 3. The red and blue triangles are the leveling data modified from [Ching et al. \(2011\)](#). The yellow squares are the 14 seismic stations from the Central Weather Bureau Seismic Network (CWBSN) and the Broadband Array in Taiwan for Seismology network (BATS); while the yellow triangles show the 8 ocean bottom seismometers (OBS) used in this study. CR: Central Range; CoR: Coastal Range; LVF: Longitudinal Valley Fault; HB: Hoping Basin; NB: Nanao Basin. The red rectangle in the inset figure shows the study area. (For interpretation of the references to color in this figure legend, the reader is referred to the web version of this article.)

marine area, which makes geophysical and geological observations difficult. Over the past few decades, several studies incorporated the Japan stations at Ryukyu Islands and some temporal Ocean Bottom Seismometer (OBS) arrays to improve the imaging of two subduction zones and showed their different characteristics ([Wu et al., 2009b](#); [Kuochen et al., 2012](#); [Theunissen et al., 2012](#); [Huang et al., 2014](#)). Their efforts and contributions were mainly dedicated on the improvement of tomographic images, which provide precise information for the understanding of local tectonic structures. Among those studies, [Theunissen et al. \(2012\)](#) have obtained 801 well-located earthquake hypocenters based on the data acquired from a three month passive experiment, which combined 22 OBSs and 51 inland stations, in the TAIGER (TAIWAN Integrated Geodynamics Research) project. However, their research on the seismicity distribution was focused on the Ryukyu forearc area. A systematically analysis for the earthquake distribution across the Taiwan area from the south to the north is still exile. In 2012, 10 Ocean Bottom Seismometers (OBSs) were deployed in the eastern Taiwan offshore area during the Across Taiwan Strait Explosion Experiment (ATSEE). This operation provides an opportunity to record the offshore seismic events with a larger coverage of seismic stations and to relocate these events with better precision. Thus, using the OBS records, in combination with the available

waveforms from the inland seismic stations and available geophysical data, we attempt to propose a better illustration for the tectonic processes occurring along the eastern coast of Taiwan.

## 2. Geological settings

Taiwan is located at the arc-continental collision region between the Luzon volcanic arc of the PSP and the continental shelf of the EP ([Fig. 1](#)) ([Ho, 1986](#); [Suppe, 1984](#)). Because of the oblique collision between the arc and the EP, the orogenic belt has been propagating southward ([Suppe, 1984](#)). Approximately 10 Ma ago, the northern Luzon arc and the southwestern Ryukyu subduction system were suggested to form a connection with a transform fault ([Lallemand et al., 2001](#)). In addition, 4 Ma ago, accompanied by a high rate of deformation, the orogeny of Taiwan began to form via the southward propagated oblique collision between the continental shelf and the Luzon volcanic arc ([Sibuet et al., 2006](#)). A portion of the arc and fore-arc sediments was accreted onto the former accretionary prism, forming the Central Range (CR) and the Coastal Range (CoR) areas ([Chang et al., 2000](#)). The Longitudinal Valley (LV) separates the CR to the west and the CoR to the east and is considered a plate boundary between the EP and the PSP. The large convergence, as indicated by the geodetic results, displays a value of  $81.5 \pm 1.3$  mm/yr in the direction of N309° ([Yu et al., 1997](#)). South of 24°N, the convergence is almost entirely distributed across the island, with a rate of 3 cm/yr accommodated in the LV area ([Angelier et al., 1997](#)).

With these complicated structures, the seismicity is largely active around Taiwan, especially in the eastern coast and the offshore area. South of 24.3°N, earthquakes in the collisional zone generally show a NW-SE compressive mechanism. Most of the  $\sigma_1$  (maximum principal stress) events can be divided to two groups,  $287^\circ \pm 10^\circ$  and  $333^\circ \pm 16^\circ$  ([Kao et al., 1998](#)), and only a few of the events have their P-axes located along the direction of plate motion ([Yu et al., 1997](#)). [Wu et al. \(2010\)](#) noticed that this variation can be associated with the depth variations. At depths shallower than 20 km, the trends of  $\sigma_1$  are roughly consistent with the convergence direction ( $333^\circ \pm 16^\circ$ ), whereas the  $\sigma_1$  rotate to  $287^\circ \pm 10^\circ$  at locations deeper than 20 km. Further north, the earthquakes separate into shallow regions and deep regions to present the opening of the Okinawa Trough and the subduction of the PSP. The shallow region contains strike-slip and normal-fault-type focal mechanisms with a NW-SE trending  $\sigma_3$  (minimal principal stress). The events occur in the deep region show a down-dipping extensional regime between 50 and 90 km in depth ([Wu et al., 2008](#)).

## 3. Methods and data

The Across Taiwan Strait Explosion Experiment (ATSEE) is a project designed to determine the structure beneath Taiwan Island and the Taiwan Strait using passive and active sources with a dense distribution of seismic stations around Taiwan. To extend the seismic array eastward, 10 ocean bottom seismometers (OBS) were deployed in the Eastern Taiwan offshore area (121.4°E–122.1°E, 22.8°N–23.7°N) from July 9 to August 3, 2012, and 8 of them were recovered ([Fig. 1](#)). The MicroOBS instruments used in the experiment, each containing one hydrophone and three component 4.5 Hz geophones as receivers, were developed by the French Research Institute for Exploitation of the Sea (Ifremer) ([Auffret et al., 2004](#)). The ATSEE project was mainly designed for wide-angle seismic experiment. The stations were deployed along the profile and the recording period was much shorter than that of the OBS network. The data from our OBS network have been integrated into the ATSEE project dataset for the velocity inversion to

understand the deep tectonic structures beneath Taiwan and across the Taiwan Strait (Kuo et al., 2015). However, the linear distribution and the short recording period of the onland seismic stations was not suitable for the determination of earthquakes distribution. Therefore, instead of incorporating the data from other ATSEE inland stations, we employed the available waveform data from the 12 inland stations in the Central Weather Bureau Seismic Network (CWBSN) and 2 stations in the Broadband Array in Taiwan for Seismology network (BATS) (Fig. 1) to improve the network geometry and enhance precision for earthquake localization. Finally, a total of 22 seismic stations, located in both the inland and offshore areas, were used for the analyses of passive seismic signals. The short-period type seismometers record a relatively smaller range of frequencies compared to that of broadband seismometers. However, the P- and S-wave arrivals used in our study were characterized by high frequency (more than 10 Hz). The use of different types of seismic stations should have no effect in the data quality (Fig. 2). Due to the limitation for the instrument autonomy, the OBSs can only record data for less than one month, 25 days in our study, which is very short with respect to the instrumental seismic observation history. However, for the tectonic active area like the eastern Taiwan, 25 days data could still provide us information about the seismologically active structures, especially in the marine area where the available seismic data is insufficient.

The application of an inappropriate velocity model in localization will cause significant errors in the earthquake position. Several seismic tomographic results are available for part of the study region (e.g. Huang et al., 2014; Kuo et al., 2012; Wu et al., 2007, 2009b). However, since our seismic network includes the inland and offshore regions, it is difficult to determine a suitable velocity model for earthquake localization. In this study, we used the double-difference relocation method (Waldhauser and Ellsworth, 2000) for the earthquake relocation. In the method, when the distance between two nearby earthquakes is much

smaller than the distance from the event to the station and the scale of the heterogeneity in the structure, the difference between travel times can be ascribed to the spatial offset between the events (Waldhauser and Ellsworth, 2000). Therefore, the effects of three-dimensional velocity structure and clock bias will be minimized. After a group of event pairs is linked together in clusters (hereafter called “the group”), the least squares solution for each cluster is found to achieve relative locations. For this purpose, the conjugate gradient algorithm LSQR (Paige and Saunders, 1982) is used to solve the damped least-square of the sparse matrix in the relocation process. After numerous tests, the spatial separation distance between two events was defined as 7 km to take both the relocation precision and the number of relocated events into consideration. We can notice that 7 km is much smaller than most of the tectonic features determined in the study, which suggests that all the structures discussed here should be reliable. The 1-D velocity model was constructed based on the model that Central Weather Bureau (CWB) uses routinely for the localization of earthquakes in Taiwan (Fig. 3a). On the other hand, the magnitudes and focal mechanisms of seismic events recognized from the seismic network were determined as well. We first calculated the magnitude using the duration of the coda wave ( $M_D$ ). Next, the local magnitudes ( $M_L$ ) of events were converted from  $M_D$  based on the empirical law proposed by Shin (1993). The focal mechanisms were determined using the first motion of P arrivals.

#### 4. Results

Based on the 25-day OBSs records, a total of 4256 P- and 5715 S-wave arrivals were manually selected, and a total of 979 earthquakes were initially located with the iasp91 global velocity model (Kennett and Engdahl, 1991) (Fig. 4a). Among these, 333 events were divided into several groups based on the distances between them and successfully relocated using the HypoDD software

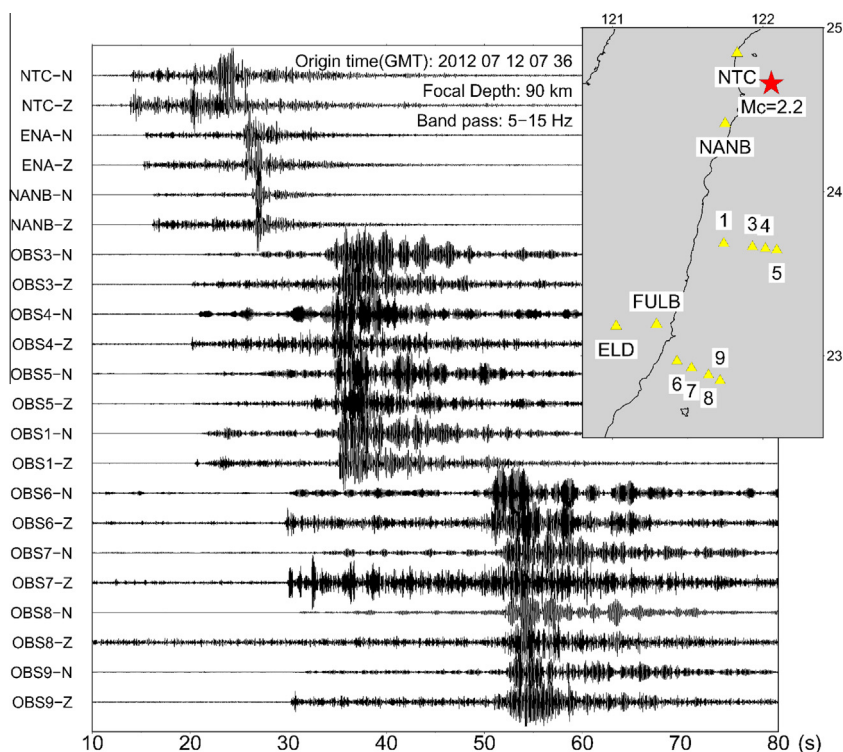


**Fig. 2.** An example of seismograms recorded by the OBSs and inland seismic stations. The inset shows the position of the recorded earthquake (red star) and the seismic stations (yellow triangles). (For interpretation of the references to color in this figure legend, the reader is referred to the web version of this article.)

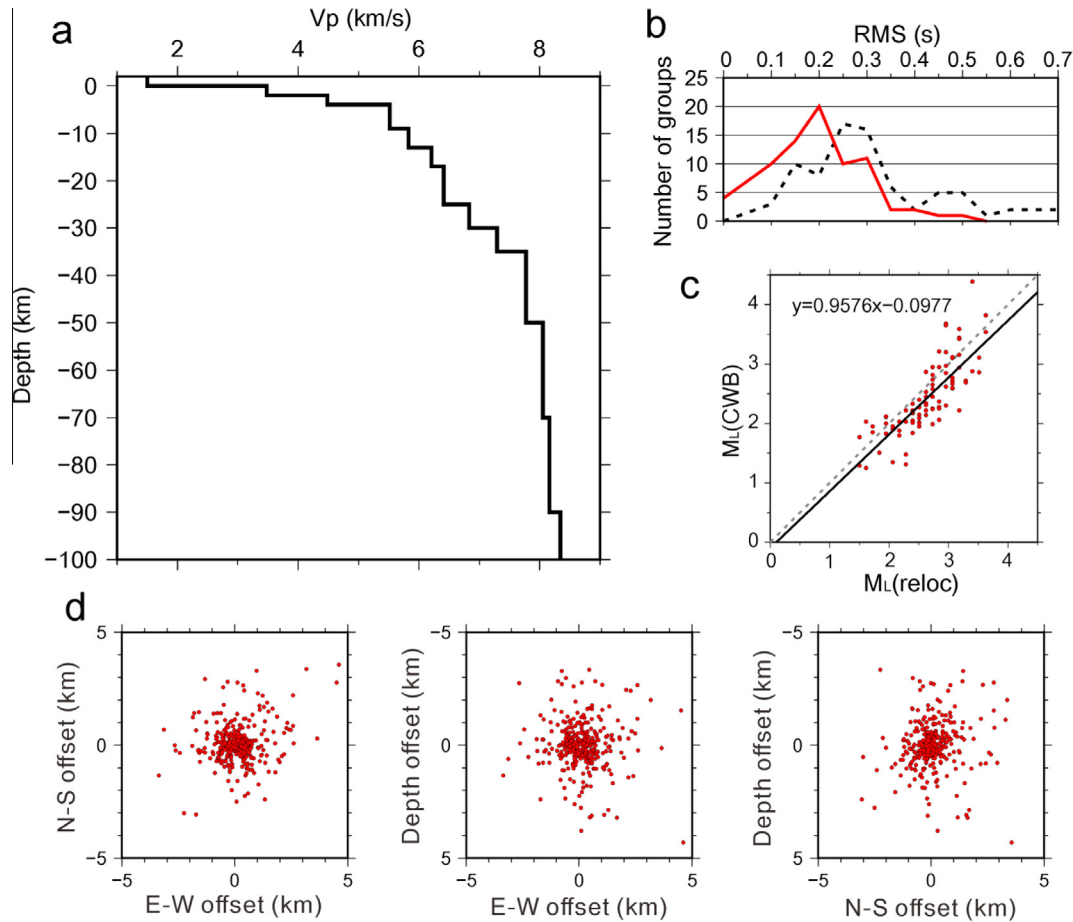


**Fig. 3.** (a) 1-D velocity model applied in the HypoDD relocation process. (b) Root-mean-squares travel time residual (RMS) of each group before (black dashed line) and after (red line) the earthquake relocation, showing an increase of the number of group with smaller RMS after the relocation. (c) Comparison of the  $M_L$  converted from the empirical law (the x-axis) and that obtained from the Central Weather Bureau (CWB) catalog (the y-axis). The solid black line denotes the regression, showing a positive correlation. The dashed line indicates the line of equality ( $y = x$ ). (d) Offsets of the relocated earthquakes location with regard to its original position in different planes. (For interpretation of the references to color in this figure legend, the reader is referred to the web version of this article.)

(Fig. 4b). Fig. 3b shows the number of the group with smaller root-mean-square travel time residual (RMS) increased after the relocation. We noticed that the number of relocated earthquakes is only approximately 34% of that in the initial localization. Such a discrepancy in number was caused by discarding of the shallow events and out-of-network events, which were too scattered to be relocated with the HypoDD method. The basic procedure behind the HypoDD relocation is to identify events that can make an event pair, and identify the station or stations that each pair can be linked to in order to make travel time corrections to that station. If no event pair was identified or insufficient information could be given for the travel time correction in each pair, the earthquakes could not be relocated by the software. More than 90% events contained offsets between the original and the relocated position less than 5 km in each direction (E-W, N-S, and vertical), and the offset pattern seems to be random without systematic effect (Fig. 3d). A comparison of the magnitude  $M_L$  converted from the  $M_D$  determined in our study and that determined by the CWB for the same event is shown in Fig. 3c. The regression of the data points (solid line in Fig. 3c) is very close to the identity line (dashed line in Fig. 3c), indicating the reliability of the magnitude determination and conversion performed in our study. Based on the first motion of certain good-quality P-wave arrivals and the fine coverage of the seismic network, 9 focal mechanism solutions with magnitude  $M_L$  between 2.8 and 3.4 were determined (Fig. 5) (Table 1). In addition, the HASH method was applied to examine the reliability of

the focal mechanisms solutions (Hardebeck and Shearer, 2002). The small fit errors and station distance ratio (STDR) indicate that the focal mechanisms solutions we defined in the study should be good enough (Table 1). Except for one NW-SE trending extensional event (No. 2 in Fig. 4b), all events are characterized by thrusting and strike-slip movement with a maximal compressional axis  $\sigma_1$  subparallel to the plate motion (Nos. 5 and 9) or along  $287^\circ \pm 10^\circ$  (Nos. 4, 7 and 8) and  $333^\circ \pm 16^\circ$  (Nos. 1, 3 and 6), as suggested by Kao et al. (1998).

After the relocalization, the distribution of seismic events appears to be more concentrated and sharpened, and most of the events are distributed along the eastern coast of Taiwan. The earthquakes are generally located at depths from 10 to 80 km and become deeper toward north (Fig. 4b). South of  $23.25^\circ\text{N}$ , earthquakes occur at a relatively shallow depth of 0–30 km and are distributed primarily along the western side of the Luzon Arc or along the southern CoR. A certain amount of seismicity is also located in the eastern flank of the arc, but no significant feature was determined. The shallowest events appear in the southern portion of CoR; by contrast, almost no events occur in the northern segment ( $\sim 23.25^\circ\text{N}$ – $24^\circ\text{N}$ ). North of  $23.25^\circ\text{N}$ , the seismic distribution is deeper than that in the south, representing a northward dipping seismic zone without the presence of shallow events. Most earthquakes strike along the eastern coast of Taiwan, whereas others are located near the northern CR, in inland Taiwan or under the Ryukyu fore-arc area. This seismicity distribution pattern is similar

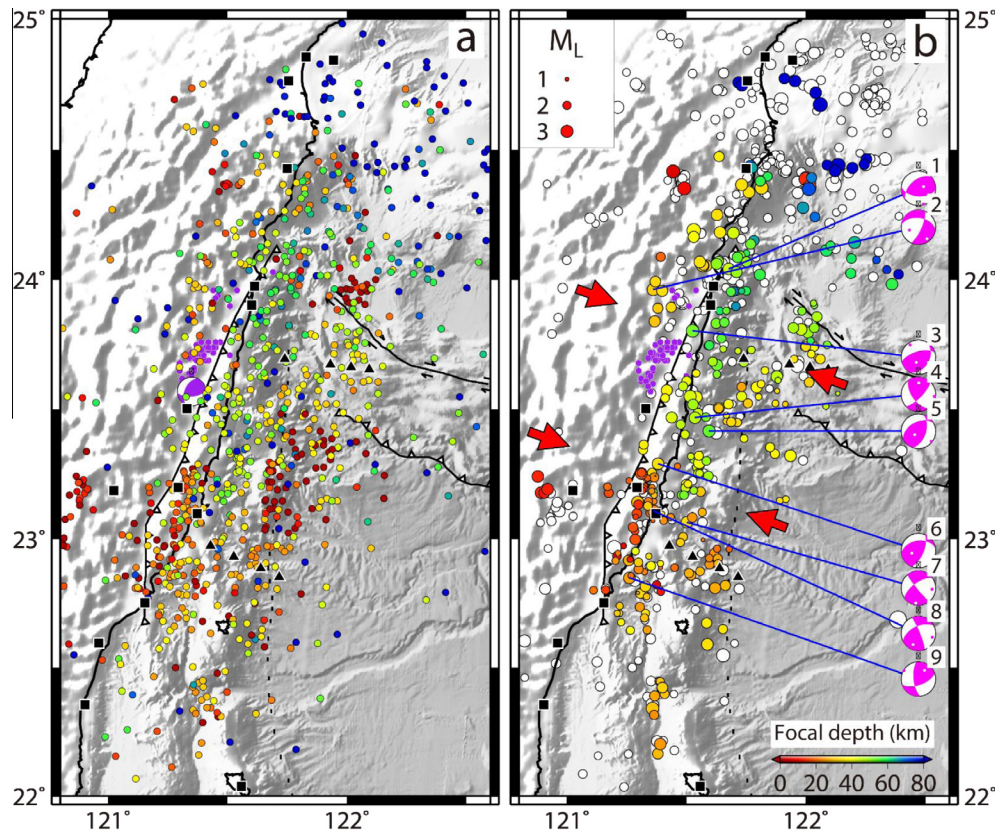


**Fig. 4.** (a) The 979 initially located earthquakes during the 25-day recorded period. (b) A total of 333 events relocated using the double-difference relocation method (Waldhauser and Ellsworth, 2000); the earthquakes from the reviewed ISC catalog are shown by the white hollow circles. The focal mechanisms in pink are determined in our study using the first motion solution. The red arrows indicate the two main boundaries suggested in our study. Purple dots represent the Ruisui earthquake sequence and the purple focal mechanism was obtained for the main shock of the Ruisui earthquake sequence. Black squares and triangles show the inland seismic stations and the OBSs. (For interpretation of the references to color in this figure legend, the reader is referred to the web version of this article.)

to those already published by the previous studies (e.g. Fig. 2 in Theunissen et al. (2012)). Notably, the discrepancy of shallow earthquakes in the area between approximately 23.25°N–24°N and the northward dipping seismic pattern could be well imaged by almost all the previous studies even though no specific discussion have been provided in the previous works. The depth of the earthquakes that occur in the island are concentrated in the range of 30–40 km. The focal mechanism determined for this seismic cluster shows an extensional nature (focal mechanism No. 2 in Fig. 2b), which differs from the focal mechanisms obtained from any other areas, indicating a different tectonic environment.

## 5. Discussion

To better examine the inland and offshore seismic activity, we projected the relocated earthquakes together with the seismic tomographic results (Kuoehen et al., 2012) along five NE-SW trending profiles, which strikes approximately in parallel with the plate boundary, LV (Fig. 6a). The onshore sections (profiles 1 and 2 in Fig. 6a) contain relatively fewer events with regard to the offshore portion (profiles 4 and 5 in Fig. 6a), which is consistent with the previous results that most earthquakes occur in the marine domain. However, the highest seismicity density appeared in the sea-land boundary, along the profile 3 (Fig. 6a and e). Based on the distribution of seismicity, two distinct boundaries, 23.25°N and 23.8°N (red arrows in Figs. 4b and 6a; black dashed lines along the five profiles shown in Fig. 6b–g), were defined to illustrate the evolution of tectonic process along the eastern Taiwan.

South of 23.25°N, the southern boundary, the earthquakes are distributed between depths of 10 and 35 km without showing any distinct feature (black dots in Fig. 6c–g). The concentration of earthquakes south of 23.25°N within a 35-km thickness suggests an ongoing collisional process, which occurs in the entire crustal portion as already suggested by previous studies (e.g. Kao and Rau, 1999; Malavieille et al., 2002). The NW-SE trending  $\sigma_1$  determined in our study (focal mechanism Nos. 7–9 in Figs. 4b and 5) and in other previous studies could also evidence this active collision. Furthermore, the area influenced by this process spreads over the inland and offshore part, mostly in the marine area. This observation suggests that the force of collision affects not only the plate boundary, such as the LV and the CoR, but also a large portion of the marine area of greater distance, including the Luzon forearc or arc cutting by the profiles 4 and 5 (Fig. 6a, f and g). Tomographic results show insignificant variation for the inland portion, where few earthquakes were observed. However, relatively larger diversity in velocity occurred in the marine area, suggesting the presence of the compressed Luzon Arc and forearc area.

North of 23.8°N, the northern boundary, the earthquakes present a clearly northward subduction pattern with a dipping angle of about 30° in the offshore profiles, which is approximately consistent with the 8 km/s velocity contour (Fig. 6e–g). The 8 km/s contour is too deep to be the top of the subducted PSP and it may represent the lower layer of the double seismic zone (Huang et al., 2014). The aseismic characteristics of the oceanic crust may be due to its highly deformed and ruptured material content or the hydrated mantle (Lallemand et al., 2013). Otherwise, a group of earthquakes trending northward with slightly smaller angle was

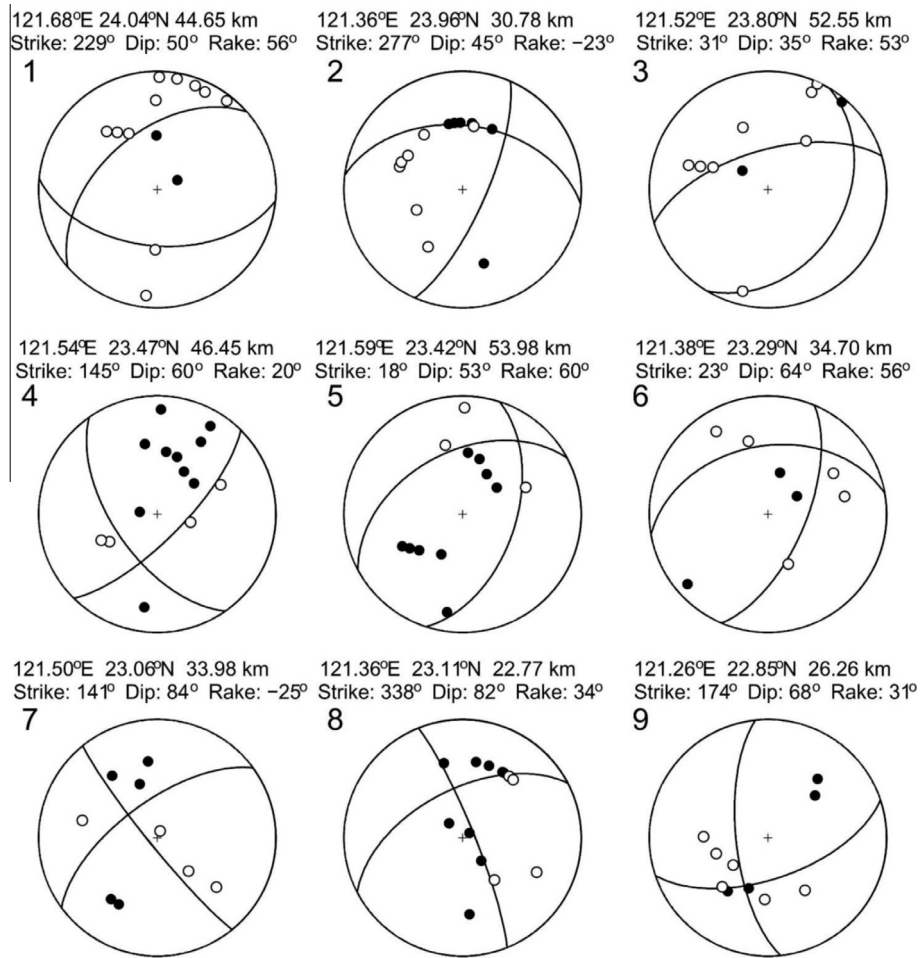


**Fig. 5.** Nine focal mechanisms determined in this study. Black and white dots represent the upward and downward first motion, respectively. Detailed information are listed in Table 1.

**Table 1**

The parameters and the HASH test result for the focal mechanisms determined from our study.

	Longitude (°)	Latitude (°)	Depth (km)	Strike (°)	Dip (°)	Rake (°)	Fit error	STDR	Fault + aux plane uncertainty (°)	
1	121.68	24.04	44.65	229	50	56	0.00	0.56	33.6	38.2
2	121.36	23.96	30.78	277	45	-23	0.09	0.81	33.3	39.0
3	121.52	23.80	52.55	31	35	53	0.21	0.52	31.2	43.4
4	121.54	23.47	46.45	145	60	20	0.00	0.68	21.6	30.6
5	121.59	23.42	53.98	18	53	60	0.00	0.78	32.0	28.7
6	121.38	23.29	34.70	23	64	56	0.00	0.69	19.3	25.8
7	121.50	23.06	33.98	141	84	-25	0.04	0.71	33.7	39.5
8	121.36	23.11	22.77	338	82	34	0.00	0.75	25.2	39.9
9	121.26	22.85	26.26	174	68	31	0.14	0.67	40.2	22.0

observed on land, along the profile 2 (Fig. 6d). This earthquake distribution can reach as far as approximately 30 km from the coast (Fig. 6a), which suggests that the PSP subduction may have entered the inland area north of 23.8°N (Lin et al., 2004; Wu et al., 1997, 2009a). The focal mechanism No. 1, possessing an approximately 30° dip angle, evidences the subduction process for this northernmost portion. We notice that the southernmost end of this feature is located at 23.8°N at depth of 25 km and becomes deeper north-eastward (Fig. 6d). No surface evidence for this subducting feature has been reported. This phenomenon could be caused by the ongoing collisional process to the south of 23.8°N which obscured the subduction-related activity.

Between 23.25°N and 23.8°N, the seismic pattern becomes more complex. The earthquakes located along the profile 3

(Fig. 6e) present northward dipping feature as in its northern portion, while those located along the profiles 4 and 5, in the offshore area (Fig. 6f and g) intensify at 35–55 km in depth without appearing any distinctive pattern. The concentration of earthquakes at depth may not be explained by the subduction-related processes of PSP because the hypocenters are much deeper than the PSP Moho (Lallemand et al., 2013), and the focal mechanisms determined in the area are uniquely characterized by NW-SE compression (focal mechanism Nos. 3–6 in Figs. 4b and 5). In the previous studies, the arc and/or forearc material was suggested to underthrust eastward along one of the conjugate fault of the Luzon volcanic arc (Chemenda et al., 1997, 2001; Malavieille et al., 2002). Based on seismic tomographic results, a relatively low velocity area, imaged at depth below 30 km, was inferred to be

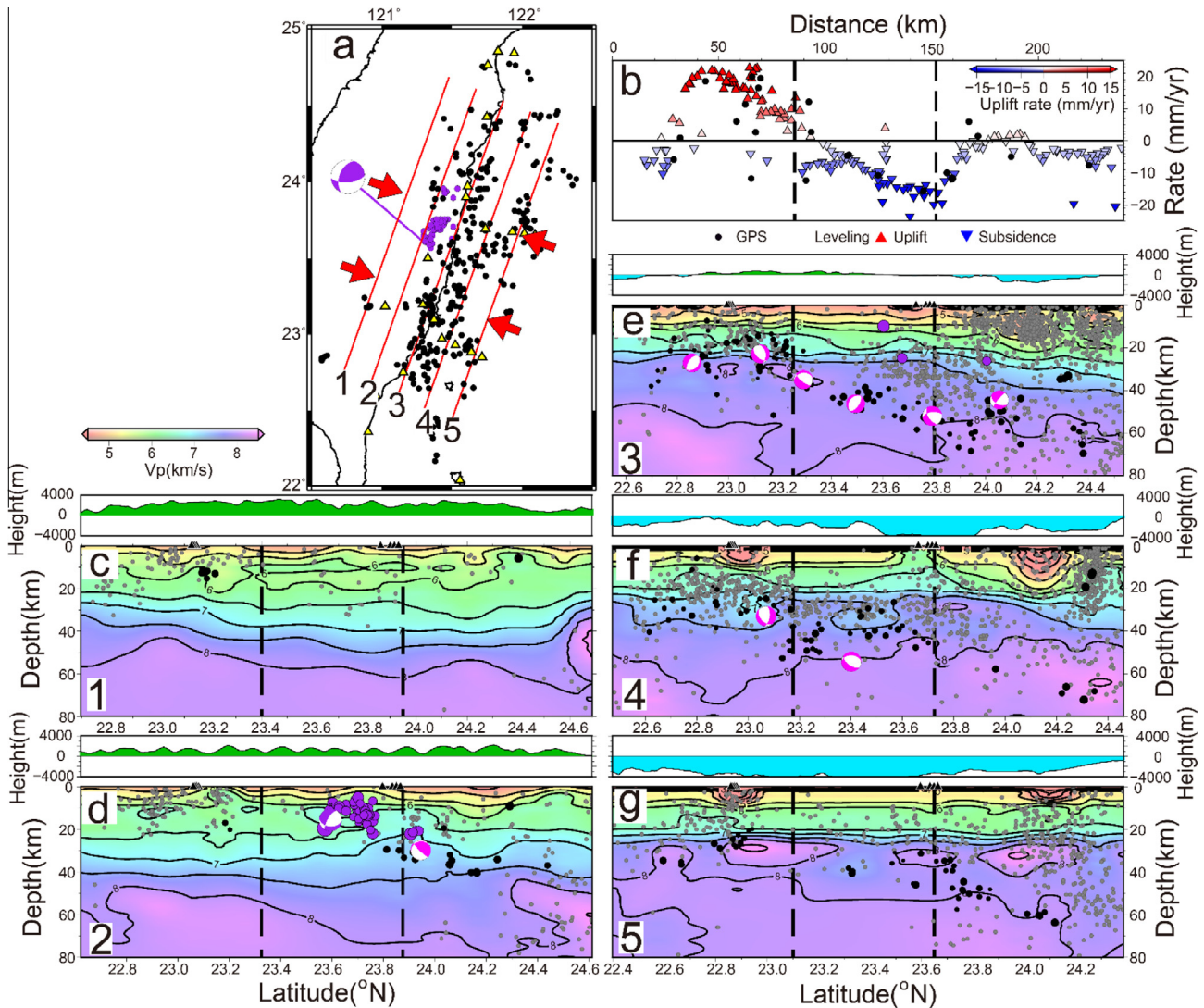


**Fig. 6.** Seismic tomographic results (Kuoehen et al., 2012) and the relocated earthquake distribution along the five NE-SW cross-sections located from the inland to offshore area. (a) Profile locations (red lines) and the relocated earthquakes (black dots) in plan view. Red arrows indicate the two main tectonic boundaries suggested in our study. (b) Leveling and continuous GPS data extracted from Ching et al. (2011). The uplift and subsidence rate calculated from the leveling experiment are shown by triangles with red and blue colors, respectively. Black dots show the vertical velocity estimated from GPS data. (c)–(g) Are the seismic tomographic results and the relocated earthquakes along the five profiles 1–5 in (a). The black dots show the relocated earthquakes. Gray dots show the earthquakes from the reviewed ISC catalog. Black dash lines indicate two tectonic boundaries. Black triangles denote the OBS positions. Purple dots and focal mechanism represent the Ruisui sequence. The pink focal mechanisms are obtained from our study. (For interpretation of the references to color in this figure legend, the reader is referred to the web version of this article.)

the underthrust arc/forearc (Huang et al., 2014; Kuoehen et al., 2012; Wu et al., 2007, 2009b). Therefore, the seismicity observed at this portion should be linked to the ongoing deformation of the arc/forearc material. In addition, only a few of earthquakes occurred to the landward side, along the profiles 1 and 2, at a distance of less than 10 km from the coast, whereas most earthquakes spread broadly in the seaward portion. This pattern should be subjected to the concentration of arc/forearc deformation in the marine area.

### 5.1. Ruisui earthquake sequence

The Ruisui  $M_L$  6.4 earthquake occurred on 31 October 2013 in the vicinity of the LV in eastern Taiwan (Figs. 4 and 6). The earthquake produced extremely strong ground motion, even people lived in Taipei City, 200 km away from the epicenter, felt the shaking for approximately 50 s. A strong motion with a peak ground acceleration larger than 400 Gal was detected in the northern LV.

Several aftershocks occurred along the NNE-SSW direction, in a good agreement with the strike of the LV. Most of them were located between 5 and 18 km in depth (Fig. 6) and shown a western dipping fault plane (Lee et al., 2014). The relocated earthquakes along the profile 2 shows a northward trending pattern (Fig. 6d), which coincided approximately with the 7 km/s velocity contour and could be linked to the northwestward subducting PSP. The shallowest relocated earthquakes occurred at approximately 25 km, and no continuation could be found from this depth to the surface. However, the position of the October 2013 Ruisui earthquake sequence extracted from CWB ([http://www.cwb.gov.tw/V7/earthquake/quake\\_index.htm](http://www.cwb.gov.tw/V7/earthquake/quake_index.htm), purple dots in Figs. 4 and 6) filled the gap from the northward trending feature to the surface, with a northwestward trending distribution, which is in a good agreement with the PSP plate motion. This connection of the deep subduction structure to the surface could be the expression for the southward propagation of the PSP subduction, which was evidenced by the spatial coincidence.

## 5.2. Comparison between the tectonic environment and the leveling data

By combining the present-day and long-term vertical velocities in Taiwan, Ching et al. (2011) found an uplift and downward movement in the southern and northern segment of the CoR, respectively (Figs. 1 and 6b). This observation was proposed to be correlated with the transition from creeping process of the LVF in the south to locking effect in the north (Ching et al., 2011). The aseismic and/or small-magnitude coseismic motion caused an uplift rate of 5–10 mm/yr in the southern part of the CoR (Hsieh and Rau, 2009), while the elastic strain accumulation produced a subsidence rate of 10–20 mm/yr in the northern portion (Huang et al., 2010). However, the consistency of the boundaries observed from the leveling data and the earthquakes distribution patterns infers that the variation of the vertical surface movement could be linked to the different tectonic processes discussed previously. The reversal of the vertical displacement rate occurs in the vicinity of 23.3°N, which corresponds to the boundary where the seismic pattern changes dramatically. South of the boundary, the earthquakes distribution shows a collisional feature which includes the entire crustal portion, and the leveling data represent an uplift process. By contrast, the leveling data become negative suddenly to the north of 23.3°N (Figs. 1 and 6b). As discussed previously, the compression of the collision-related effect may force the arc/fore-arc material to move downward, which could cause the surface subsidence on the leveling observation. Furthermore, the uplift rate dropped substantially at 23.3°N and remained at a value lower than approximately –15 mm/yr between 23.6°N and 23.85°N. This segment of relative more rapid subsidence rate coincided with the location of the October 2013 Ruisui earthquakes sequence, inferring the potential correlation between the occurrences of subduction-related earthquakes and the surface vertical velocity in this area. To the north of 23.85°N, where the northward dipping seismic pattern was obviously presented, the uplift rate returned to almost neutral.

## 6. Conclusion

Even though numerous seismic tomographic and seismicity relocation studies have been performed for the understanding of the ongoing tectonic processes along the eastern Taiwan, a continuous analysis of the spatial distribution of seismicity from the south to the north of Taiwan from a broad view seems insufficient. Based on the seismicity recorded from 22 onshore and offshore seismometers, we relocated 333 earthquakes by using the double-difference relocation method to obtain a more detailed and accurate distribution of earthquakes along the eastern Taiwan. Based on the continuously spatial examination on the relocated events from the south to the north, we suggest that two main boundaries divide the eastern Taiwan into different areas with distinct ongoing tectonic processes. The boundary for the collision and the transition zones appears at ~23.25°N. South of this boundary, all the earthquakes spread homogeneously in the crustal portion, expressing an arc-continental collisional process. The transition from the collision to subduction along the eastern Taiwan should concentrate in the area between 23.25°N and 23.8°N, where the arc/fore-arc block deformed at depth as revealed by the dramatically deepening of hypocenters. North of 23.8°N, the northwest-dipping PSP is well illustrated by seismicity in both the onshore and offshore areas. Even though the two boundaries were defined clearly in our study, the October 2013 Ruisui earthquakes sequence connected the northward dipping feature at 23.8°N to the shallower part at 23.6°N, suggesting the south prolongation of the subduction-related mechanism. This observation

could infer the co-existence of collisional and subduction process in this transition portion.

## Acknowledgement

We thank the Geophysical Database Management System (GDMS) of Central Weather Bureau (CWB) for providing high quality data (Shin et al., 2013). All figures were made by the Generic Mapping Tools (Wessel and Smith, 1998). This research was supported by the Taiwan Earthquake Research Center (TEC) funded through the Ministry of Science and Technology, Taiwan (MOST) with grant MOST-104-2811-M-008-029 and MOST-104-3113-M-008-001.

## References

- Angelier, J., Chu, H.-T., Lee, J.-C., 1997. Shear concentration in a collision zone: kinematics of the Chihshang Fault as revealed by outcrop-scale quantification of active faulting, Longitudinal Valley, eastern Taiwan. *Tectonophysics* 274, 117–143.
- Auffret, Y., Pelleau, P., Klingelhoefer, F., Geli, L., Crozon, J., Lin, J.-Y., Sibuet, J.-C., 2004. MicroOBS: a new generation of ocean bottom seismometer. *First Break* 22, 41–47.
- Chang, C.P., Angelier, J., Huang, C.Y., 2000. Origin and evolution of a melange: the active plate boundary and suture zone of the Longitudinal Valley, Taiwan. *Tectonophysics* 325, 43–62.
- Chemenda, A.L., Yang, R.-K., Hsieh, C.-H., Groholsky, A.L., 1997. Evolutionary model for the Taiwan collision based on physical modeling. *Tectonophysics* 274, 253–274.
- Chemenda, A.L., Yang, R.-K., Stephan, J.-F., Konstantinovskaya, E.A., Ivanov, G.M., 2001. New results from physical modelling of arc-continent collision in Taiwan: evolutionary model. *Tectonophysics* 333, 159–178.
- Ching, K.-E., Hsieh, M.-L., Johnson, K.M., Chen, K.-H., Rau, R.-J., Yang, M., 2011. Modern vertical deformation rates and mountain building in Taiwan from precise leveling and continuous GPS observations, 2000–2008. *J. Geophys. Res.* 116, B08406. <http://dx.doi.org/10.1029/2011JB008242>.
- Hardebeck, J.L., Shearer, P.M., 2002. A new method for determining first-motion focal mechanisms. *Bull. Seismol. Soc. Am.* 92, 2264–2276.
- Ho, C.S., 1986. A synthesis of the geologic evolution of Taiwan. *Tectonophysics* 125, 1–16.
- Hsieh, M.-L., Rau, R.-J., 2009. Late Holocene coseismic uplift on the Hua-tung coast, eastern Taiwan: evidence from mass mortality of intertidal organisms. *Tectonophysics* 474, 595–609.
- Huang, H.-H., Wu, Y.-M., Song, X., Chang, C.-H., Lee, S.-J., Chang, T.-M., Hsieh, H.-H., 2014. Joint Vp and Vs tomography of Taiwan: implications for subduction-collision orogeny. *Earth Planet. Sci. Lett.* 392, 117–191.
- Huang, W.-J., Johnson, K.M., Fukuda, J.I., Yu, S.-B., 2010. Insights into active tectonics of eastern Taiwan from analyses of geodetic and geologic data. *J. Geophys. Res.* 115, B03413. <http://dx.doi.org/10.1029/2008JB006208>.
- Kao, H., Shen, S.-s.j., Ma, K.-F., 1998. Transition from oblique subduction to collision: earthquakes in the southernmost Ryukyu arc-Taiwan region. *J. Geophys. Res.* 103, 7211–7229.
- Kao, H., Rau, R.-J., 1999. Detailed structures of the subducted Philippine Sea plate beneath northeast Taiwan: a new type of double seismic zone. *J. Geophys. Res.* 104, 1015–1033.
- Kennett, B.L.N., Engdahl, E.R., 1991. Traveltimes for global earthquake location and phase identification. *Geophys. J. Int.* 105, 429–465.
- Kuo, Y.-W., Wang, C.-Y., Kuochen, H., Jin, X., Cai, H.-T., Lin, J.-Y., Wu, F.T., Yen, H.-Y., Huang, B.-S., Liang, W.-T., Okaya, D., Brown, L., 2015. Crustal structures from the Wuyi-Yunkai orogen to the Taiwan orogen: the onshore-offshore wide-angle seismic experiments of the TAIGER and ATSEE projects. *Tectonophysics*.
- Kuochen, H., Wu, F.T., Roecker, S.W., 2012. Three-dimensional P velocity structures of the lithosphere beneath Taiwan from the analysis of TAIGER and related seismic data sets. *J. Geophys. Res.* 117, B06306. <http://dx.doi.org/10.1029/2011JB009108>.
- Lallemant, S., Font, Y., Bijwaard, H., Kao, H., 2001. New insights on 3-D plates interaction near Taiwan from tomography and tectonic implications. *Tectonophysics* 335, 229–253.
- Lallemant, S., Theunissen, T., Schnürle, P., Lee, C.-S., Liu, C.-S., Font, Y., 2013. Indentation of the Philippine Sea plate by the Eurasia plate in Taiwan: details from recent marine seismological experiments. *Tectonophysics* 594, 60–79.
- Lee, S.-J., Huang, H.-H., Shyu, J.B.H., Yeh, T.-Y., Lin, T.-C., 2014. Numerical earthquake model of the 31 October 2013 Ruisui, Taiwan, earthquake: source rupture process and seismic wave propagation. *J. Asian Earth Sci.* 96, 374–385.
- Lin, J.-Y., Hsu, S.-K., Sibuet, J.-C., 2004. Melting features along the western Ryukyu slab edge (northeast Taiwan): tomographic evidence. *J. Geophys. Res.* 109, B12402. <http://dx.doi.org/10.1029/2004JB003260>.
- Lu, C.-Y., Angelier, J., Chu, H.-T., Lee, J.-C., 1995. Contractional, transcurrent, rotational and extensional tectonics: examples from Northern Taiwan. *Tectonophysics* 246, 129–146.

- Malavieille, J., Lallemand, S.E., Dominguez, S., Deschamps, A., Lu, C.-Y., Liu, C.-S., Schnurle, P., Crew, A., 2002. Arc-continent collision in Taiwan: new marine observations and tectonic evolution. *Spec. Pap. – Geol. Soc. Am.*, 187–211.
- Paige, C.C., Saunders, M.A., 1982. LSQR: an algorithm for sparse linear equations and sparse least squares. *ACM Trans. Math. Softw. (TOMS)* 8, 43–71.
- Shin, T.-C., 1993. The calculation of local magnitude from the simulated wood-Anderson seismograms of the short-period seismograms in the Taiwan area. *Terr. Atmos. Ocean. Sci.* 4, 155–170.
- Shin, T.-C., Chang, C.-H., Pu, H.-C., Lin, H.-W., Leu, P.-L., 2013. The geophysical database management system in Taiwan. *Terr. Atmos. Ocean. Sci.* 24, 8.
- Sibuet, J.-C., Hsu, S.-K., Normand, A., 2006. Tectonic significance of the Taitung Canyon, Huatung Basin, east of Taiwan. *Mar. Geophys. Res.* 27, 77–79.
- Suppe, J., 1984. Kinematics of arc-continental collision, flipping of subduction and back-arc spreading near Taiwan. *Mem. Geol. Soc. China* 6, 21–33.
- Theunissen, T., Lallemand, S., Font, Y., Stephanie, G., Lee, C.-S., Liang, W.-T., Wu, F.T., Theo, B., 2012. Crustal deformation at the southernmost part of the Ryukyu subduction (East Taiwan) as revealed by new marine seismic experiments. *Tectonophysics* 578, 10–30.
- Ustaszewski, K., Wu, Y.-M., Suppe, J., Huang, H.-H., Chang, C.-H., Carena, S., 2012. Crust–mantle boundaries in the Taiwan-Luzon arc-continent collision system determined from local earthquake tomography and 1D models: implications for the mode of subduction polarity reversal. *Tectonophysics* 578, 31–49.
- Waldhauser, F., Ellsworth, W.L., 2000. A double-difference earthquake location algorithm: method and application to the northern Hayward fault, California. *Bull. Seismol. Soc. Am.* 90, 1353–1368.
- Wessel, P., Smith, W.H.F., 1998. New, improved version of generic mapping tools released. *EOS Trans. Am. Geophys. Union*, 79.
- Wu, F.T., Liang, W.-T., Lee, J.-C., Benz, H., Villasenor, A., 2009a. A model for the termination of the Ryukyu subduction zone against Taiwan: a junction of collision, subduction/separation, and subduction boundaries. *J. Geophys. Res.*, 114.
- Wu, F.T., Rau, R.-J., Salzberg, D., 1997. Taiwan orogeny: thin-skinned or lithospheric collision? *Tectonophysics* 274, 191–220.
- Wu, Y.-M., Chang, C.-H., Zhao, L., Shyu, J.B.H., Chen, Y.-G., Sieh, K., Avouac, J.-P., 2007. Seismic tomography of Taiwan: improved constraints from a dense network of strong motion stations. *J. Geophys. Res.* 112, B08312. <http://dx.doi.org/10.1029/2007JB004983>.
- Wu, Y.-M., Hsu, Y.-J., Chang, C.-H., Teng, L.S., Nakamura, M., 2010. Temporal and spatial variation of stress field in Taiwan from 1991 to 2007: insights from comprehensive first motion focal mechanism catalog. *Earth Planet. Sci. Lett.* 298, 306–316.
- Wu, Y.-M., Zhao, L., Chang, C.-H., Hsu, Y.-J., 2008. Focal-mechanism determination in Taiwan by genetic algorithm. *Bull. Seismol. Soc. Am.* 98, 651–661.
- Wu, Y.M., Shyu, J.B.H., Chang, C.H., Zhao, L., Nakamura, M., Hsu, S.-K., 2009b. Improved seismic tomography offshore northeastern Taiwan: implications for subduction and collision processes between Taiwan and the southernmost Ryukyu. *Geophys. J. Int.* 178, 1042–1054.
- Yu, S.-B., Chen, H.-Y., Kuo, L.-C., 1997. Velocity field of GPS stations in the Taiwan area. *Tectonophysics* 274, 41–59.